ELSEVIER

Materials Science and Engineering A340 (2003) 272–280

MATERIALS SCIENCE & ENGINEERING A

www.elsevier.com/locate/msea

Lattice strain evolution in IMI 834 under applied stress

Mark R. Daymond [a,*], Neil W. Bonner [b]

[a] *ISIS Facility, Rutherford Appleton Laboratory, Chilton, Didcot, Oxfordshire OX11 0QX, UK*
[b] *Rolls Royce plc., PO Box 31, Derby DE24 8BJ, UK*

Received 11 December 2001; received in revised form 20 March 2002

Abstract

The effect of elastic and plastic anisotropy on the evolution of lattice strains in the titanium alloy IMI834 has been examined during a uniaxial tensile test, by in situ monitoring on the Engin instrument at the ISIS pulsed neutron source. Measurements were made at load during an incremental loading test. The data is analysed in the light of the requirements for engineering residual stress scanning measurements performed at polychromatic neutron and synchrotron diffraction sources. Comparisons between the measured strains from different lattice families and the predictions from an elasto-plastic self-consistent model are made. Agreement is good in the elastic regime and for most diffraction planes in the plastic regime.

Keywords: Titanium; Lattice strain; Residual strain; Intergranular strain; Neutron diffraction; Rietveld refinement; Self-consistent model

1. Introduction

Titanium is a reasonably common structural material, with high specific strength and stiffness at room temperature. At present its uses are limited to advanced applications due to the cost of producing the pure metal, although new production techniques [1] hold out the hope of significant cost reductions in the future. Its properties continue to be excellent at the elevated temperatures found in the intermediate stages of jet engines. In order to produce the required end-use components, the material is forged, heat treated and machined, before typically either welding of pre-shaped components [2,3], or machining of larger blanks [4] is required. In each case the processing will introduce or modify residual stresses that may remain to some extent even after further stress relieving heat treatments.

One highly successful experimental technique, which is ideal for non-destructive scanning of internal strain, is diffraction by either neutrons or synchrotron radiation. Neutron diffraction relies on the same physics as the analogous measurement of stress using laboratory based X-rays [5], but neutrons have one principal benefit for the engineer or materials scientist. That is, since neutrons interact primarily with the nucleus, rather than the electron cloud as X-rays do, the penetration depth of neutrons is very large compared with X-rays of comparable wavelength. This results in neutrons being a suitable probe for the measurement of bulk average material properties. For many practical applications, it is these bulk averaged properties in which the engineer or materials scientist is primarily interested in.

In diffraction strain measurement, changes in the separation of one or more suitably orientated crystallographic lattice planes are monitored. The technique measures the interatomic lattice spacing and is thus a direct measure of *elastic* strain and hence with a knowledge of the appropriate stiffness, the stress can be calculated [5]. When most materials are mechanically loaded, individual lattice planes will strain to different extents both with respect to each other, and to the continuum macrostrain (e.g. [6]). Individual grains exhibit elastic stiffness anisotropy, commonly treated through the use of plane specific diffraction elastic constants, but plastic anisotropy is also evident as plastic relaxation occurs preferentially on certain slip systems. It is important to understand the mechanisms of interaction between differently orientated crystallites,

* Corresponding author. Tel.: +44-1235-445434; fax: +44-1235-445720
E-mail address: mark.daymond@rl.ac.uk (M.R. Daymond).

0921-5093/02/$ - see front matter
PII: S0921-5093(02)00183-1

as a materials scientist interested in the mechanics of polycrystalline plasticity, but also as an engineer wishing to use diffraction as a tool for stress measurement. Despite increasingly sophisticated models of polycrystalline plasticity (e.g. [7]), we are far from predicting quantitatively the evolution of grain orientation dependent strains in all cases, or the implications of their spread and development on failure. The use of self-consistent models does give some insight into polycrystalline plasticity, and is therefore, a useful tool for interpreting such diffraction data.

This paper describes in situ loading measurements on IMI834. The alloy is considered to be entirely alpha phase titanium, i.e. hexagonal close packed, and was developed for use in aeroengines during the 1980s. A number of position sensitive diffraction based strain measurements have been made on titanium components [2–4], and in each case concerns have been raised about the effect of intergranular strains (i.e. strains introduced due to anisotropy between different grains) on the interpretation of these results. Other experiments have considered residual intergranular strains introduced subsequent to applied plastic strains at zero load [8]; here we consider strains measured at applied load.

At monochromatic sources, the practical approach to deal with plastic anisotropy is to define a suitable (individual) plane for macrostrain scanning as one that is little affected by intergranular strains, i.e. one whose response remains linear with increasing applied or residual stress. This is necessary since it is often impractical to measure multiple reflections. At neutron time-of-flight or energy dispersive X-ray sources, however, a diffraction pattern is recorded over a range of lattice spacings; thus many diffraction peaks are recorded. Accordingly, it is usual to fit the entire diffraction pattern simultaneously using a Rietveld or Pawley refinement, thus providing lattice parameter(s) which represent an average over all the diffraction peaks. Such an approach has been found to be relatively insensitive to intergranular effects [9,10]; the approaches discussed for austenitic steel and beryllium in these papers are applied here to titanium.

2. Experimental method

At a time-of-flight neutron source such as ISIS, neutron pulses with a continuous range of wavelengths are directed at a specimen. The time taken for diffracted neutrons to reach the detectors are measured, allowing calculation of their wavelengths, and the recording of diffraction spectra. A range of lattice planes is, therefore, examined in each measurement. It is important to note that the scattering vectors for all the reflections recorded in a particular detector lie in the same direction relative to the sample. Each reflection is produced from a different family of grains, oriented such that a specific lattice plane diffracts to the detector, and represents the average lattice spacing in the irradiated volume of the suitable oriented grains. A more complete description of these issues can be found elsewhere [11]. While it is possible to carry out fits to individual peaks within the collected spectrum, typically the whole spectrum is fitted simultaneously using a Rietveld refinement [12]. In the Rietveld method a crystal structure is proposed, from which a predicted diffraction spectrum is compared with the measured pattern. The idealised structure is then optimised in a least-squares manner to maximise the agreement between prediction and measurement. The advantage of using this approach is that measurements are more rapid than would be possible using a single peak analysis, and that the strains obtained are felt to be less sensitive to the effects of plasticity. While for an unstrained polycrystal the merit of this approach is clear, complications arise within a solid polycrystalline material. The displacements of the individual lattice reflections (relative to an unstrained reference) depend on the elasto-plastic history of the polycrystal, which itself will be affected by local effects such as texture. The peak positions of the distorted polycrystal will, therefore, deviate from an isotropic ideal, although the deviation from the nominal powder crystal structure has a relatively small effect on the absolute lattice parameter, and is insufficient to preclude convergence of the fit. The individual lattice plane strains predicted by such a refinement will thus be over- or under-estimates, dependent on the behaviour of that plane relative to the mean Rietveld strain response. The magnitude of the disparities will depend on the level of deformation and on the degree of anisotropy for the material in question. One explanation for the empirical observation of linearity in the Rietveld strain response in the plastic regime lies in a load sharing argument; when one grain undergoes slip and unloads, other grains must bear a greater part of the load increment, in analogy with two phase composite deformation. By producing a lattice parameter, which is appropriately averaged over many grain orientations, a linear response is obtained in the plastic regime. The break down in the load sharing argument comes in that we measure elastic strain, not stress, and hence changes in Poisson constraints will influence the results. However, we argue that in producing a measurement averaged over many lattice planes, the response is representative of the average bulk response in which in many cases the engineer is most interested. On the other hand, plasticity mechanisms can be directly investigated by monitoring the deviation of lattice plane responses from linearity.

The experimental loading rig and its use on the Engin beamline at the ISIS neutron source is described in some detail in [13]. In brief, the stress rig is mounted with its loading axis oriented horizontally and at 45° to the

incident beam, with two detectors oriented at $\pm 90^\circ$ to this beam. Strain components are thus determined parallel and perpendicular to the applied load. The incident beam height and width were defined as 5×5 mm using slits, while the diffracted beam width is defined to be 1.5 mm using radial collimators. The typical measurement time per load level was 2–3 h.

Tensile specimens with a diameter of 5.6 mm were machined from a disc forging of IMI834 (nominally by weight Al 5.6%, 4% Sn, 3.6% Zr, 0.7% Nb, 0.5% Mo, 0.05% C, balance Ti). After forging the disc was solution treated, aged and air cooled, with the specimen axis then cut tangentially to the disc. The diffraction data confirmed that the sample had an approximately random texture. The specimen was loaded incrementally and neutron data were measured at constant applied load. Above the elastic limit, relaxation was observed in the material, that is the macroscopic strain increased while the specimen was being held at constant load. One approach to avoid this problem is to load and immediately to unload the sample [8], thus studying just the residual strains remaining after a given increment of plastic deformation, at zero applied load. However, as in many materials, reverse yielding was observed during the unloading of IMI834 after plastic deformation; while the unloading of the material is initially elastic, as the applied stress approaches zero, inelastic effects are observed in the macroscopic response (see Fig. 1, below 100 MPa). Measurement of residual strains will thus not allow the separation of any reverse plasticity effects from those due to loading. Here, the measurement has been carried out at constant load; the macroscopic strains indicated in Fig. 1 are the averages at each loading point. On the other hand, these measurements suffer in that continuous elongation or creep occurred during the measurement, which may influence the measured lattice strains. Both fits to single diffraction peaks, and Rietveld refinement analyses have been performed.

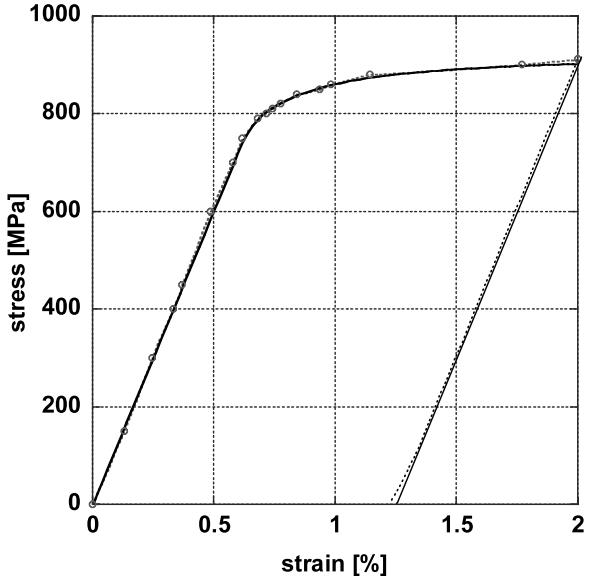

Fig. 1. Comparison between measured (broken) and modelled (continuous) macroscopic stress–strain response. Points indicate average strain during neutron measurement.

3. Self-consistent model

We have utilised the elasto-plastic self-consistent model described in more detail in [14]. In brief, this model utilises the Hill self-consistent approach [15], which was first implemented by Hutchinson [16] to describe the elastic/plastic properties of a polycrystalline aggregate. As inputs, the model requires a population of grains, chosen with a distribution of orientations and volume fractions that match the measured texture. Each grain in the model is treated as a spherical inclusion with anisotropic elastic constants and slip mechanisms characteristic of a single crystal of the material. Interactions between individual grains and the surrounding medium, which has properties that represent the average of all the grains, are performed using an elasto-plastic Eshelby type self-consistent formulation. Since the properties of the medium derive from the average response of all the grains, these are initially undetermined and must be solved by iteration. Small total deformations are assumed (typically less than 4%), and no lattice rotation or texture development is incorporated in the model. Implicit in the model formulation, no account is taken of nearest neighbour interaction nor local microstructure effects, however some considerable success has been achieved using these models to describe polycrystalline plasticity as investigated by diffraction (e.g. [7,13,14,17,18]).

The single crystal elastic constants for pure α-Ti were obtained from literature values [19], but in order that the model match the observed macroscopic modulus, values 4.8% higher were used (thus $C_{11} = 167.7$, $C_{33} = 189.8$, $C_{44} = 48.7$, $C_{12} = 94.3$ and $C_{13} = 69.2$ GPa). This is in line with the observation that the diffraction elastic constants of IMI-834 are $\sim 5\%$ higher than those of pure α-Ti [3]. Firstly, slip was modelled, in order of decreasing ease, on the prismatic, pyramidal and basal planes [20], however with only these three modes present, the modelled macroscopic response was far stiffer in the plastic regime than that observed experimentally. A number of twinning modes have also been reported in pure titanium [21], and in order to reproduce the correct macroscopic response three twinning modes are required; namely the $\{10\bar{1}2\}$, $\{11\bar{2}1\}$ and $\{11\bar{2}2\}$ type twins. However, recent descriptions [22,23] of the deformation modes acting in Ti alloys with significant Al concentration, such as that found in IMI834, suggest that $\langle c+a \rangle$ slip is a preferred deformation mode to

twinning. Thus we have used $\langle c+a \rangle$ slip here, although we also show some results obtained when including twinning in the model. When used, twinning is treated in the model in a similar manner to plastic slip, with twins characterised by their plane and direction and with a critical resolved shear stress (CRSS) and a hardening description [18]. This approach, therefore, does not include grain reorientation, stress relaxation, the change in preferred orientation due to twinning nor any changes in constraint due to the presence of a twin boundary. Despite this simplistic approach, the model does provide further relaxation modes, which greatly improves its applicability to many materials. The contribution of various deformation modes to the observed residual strain distributions is discussed in [8]. The CRSS and hardening behaviour are defined for each of the relaxation mechanisms and are varied as fitting parameters to give optimum agreement between the measured and predicted macroscopic stress-strain curves (see Table 1). The hardening function used for each system is described in detail in [13]. In this work an isotropic hardening model was used with latent hardening equal to self-hardening, and with equal hardening interactions between each relaxation mode. With several relaxation mechanisms available, one can argue that obtaining agreement with the macroscopic curve is unlikely to be a unique solution, therefore, the following constraints were placed on the CRSS and hardening behaviour; (a) the CRSS increases in magnitude from prism⇒pyramidal⇒basal⇒$\langle c+a \rangle$ modes, as reported elsewhere, and (b) all slip modes have the same hardening behaviour. In [22], $\langle c+a \rangle$ slip was observed on the $\langle 11\bar{2}3 \rangle\{10\bar{1}1\}$ system, with secondary slip often observed on $\langle 11\bar{2}3 \rangle\{11\bar{2}2\}$. However including both of these modes had negligible impact on the intergranular strain response predicted, compared with when including only the primary $\langle 11\bar{2}3 \rangle\{10\bar{1}1\}$ mode and hence we have used this latter approach. While it is unlikely in the extreme that all the above assumptions are completely valid, they simplify and constrain the problem, and although undoubtedly further independent adjustment of the various parameters could improve the agreement between the model and the experiment, the extent to which valid conclusions could be drawn is unclear given the assumptions implicit in the model. The model was run with 1000 randomly oriented grains.

The detectors on ENGIN subtend 14° at the sample, thus a diffraction spectrum in 2θ that is integrated over the whole detector corresponds to an average over $\pm$ 3.5° in strain orientation in θ at the sample [24]. In order to compare the model with the experiment, a subset of the total population of grains used in the model is identified for each diffracting family, defined by the condition that the lattice plane normal lies within a similar angular interval of the loading axis, or the direction perpendicular to it. These are the grains that would contribute to a diffraction measurement of strain in that direction, and an average of the lattice plane strain for each subset of grains is compared with the neutron results below.

Table 1
CRSS for deformation modes

Mode	Prismatic	Pyramidal	Basal	$\langle c+a \rangle$
CRSS (MPa)	310	340	390	430

4. Evolution of lattice strains

Fig. 2 compares the lattice strains measured parallel to the applied load with the model predictions for a number of 1st order diffraction peaks [25]. Firstly, the responses demonstrate the relatively low elastic anisotropy of IMI834, with the various single peak strains behaving similarly in the elastic regime. It is not simple to compare quantitatively crystallographic elastic anisotropy in cubic and hexagonal materials, but this can be done in an empirical manner defining the parameter r as

$$r = \frac{E_{\text{stiff}} - E_{\text{compliant}}}{(E_{\text{stiff}} + E_{\text{compliant}})/2} \quad (1)$$

where E_{stiff} is the polycrystalline modulus along the stiffest crystallographic direction (e.g. 0002 in Ti, 111 in cubic materials), and $E_{\text{compliant}}$ corresponds to the most compliant crystallographic direction. We obtain values for stainless steel of $r = 0.45$ and for aluminium of $r = 0.15$, materials typically considered to have large and negligible elastic anisotropy, respectively [26]. The corresponding value for titanium is $r = 0.16$. Given, therefore, that a small range of elastic anisotropy is expected, the model captures the observed differences very well.

Once plasticity occurs, at around 780 MPa, the single peak responses deviate from linearity (Fig. 2). Various grain families require different applied stresses to initiate deformation, firstly since the induced internal stress in each grain varies due to differing stiffnesses as described above, and secondly since the relative orientation of the grains to the loading axis will enhance or diminish the likelihood of slip. Once slip occurs in particular preferentially oriented grains, load will be transferred from this family to other grains less favourably oriented for slip. Strain will continue to accumulate in grains, which have yielded, since they will harden, but at a lower rate than in the elastic regime. Hence, in a manner analogous to the transfer of load in a two phase composite [27], the lattice planes with indices $10\bar{1}2$ and $10\bar{1}3$ are preferentially unloaded, while correspondingly the $10\bar{1}0$ plane is loaded as the former planes relax. The thick lines in Fig.

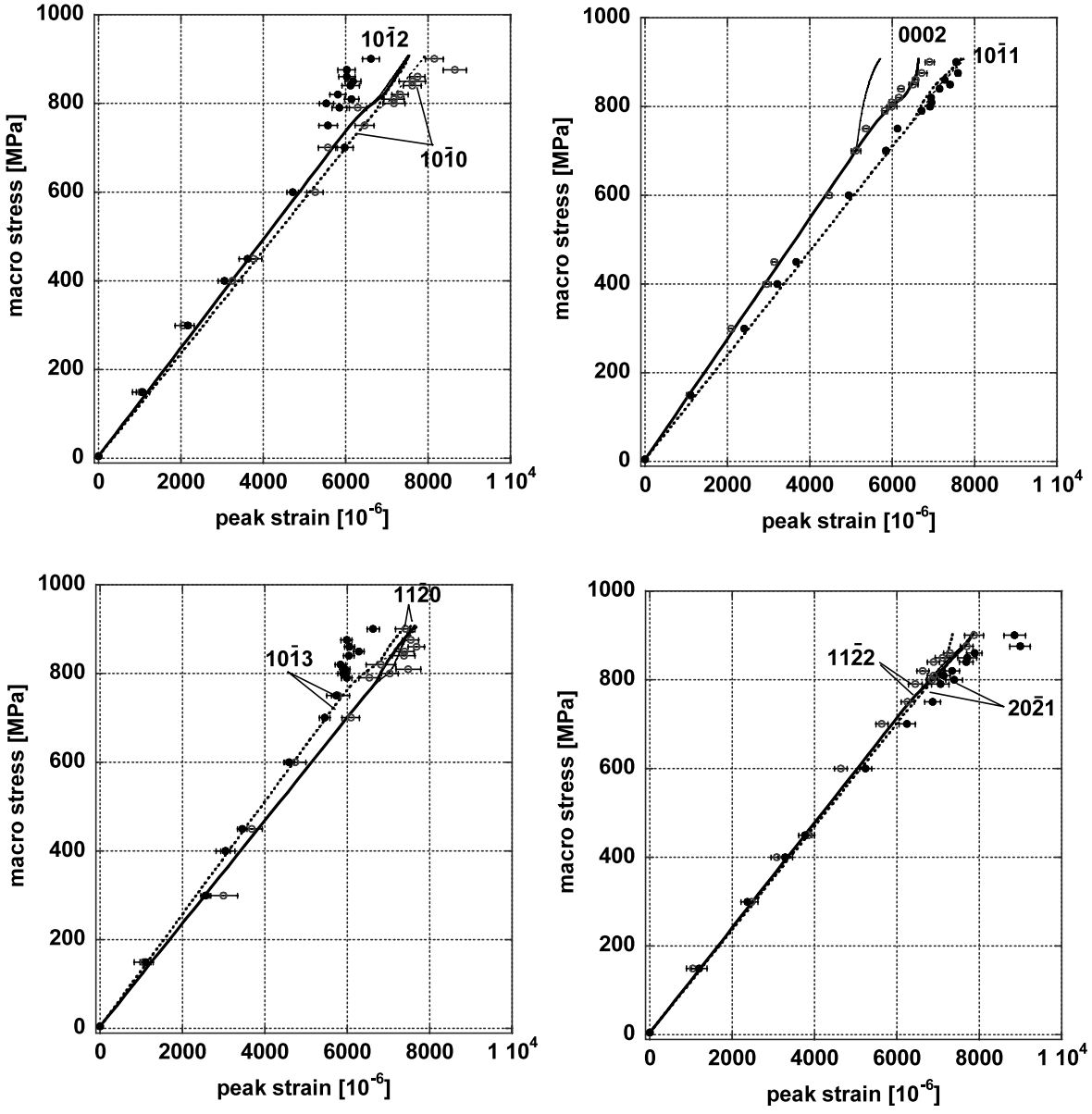

Fig. 2. Single peak axial strains compared with model predictions. Thick lines are for the model run with four slip modes, the thin lines for the model run with three slip modes and three twinning modes.

2 indicate the model predictions using four slip modes, while for comparison we also use thin lines to indicate predictions from the model using three slip modes and twinning. The model captures several of the load transfer features quite well, however there are clear discrepancies between model and experiment for the 10$\bar{1}$2 and 10$\bar{1}$3 planes which in fact unload yet are predicted by the model to be relatively weakly affected by macroscopic yielding. The 0002 oriented grains are the only family where a significant difference is seen between predictions from the two models. Experimentally there is a slight transfer of load to the 0002 grains. The reverse is predicted for the model including twinning, while for the model using four slip modes the direction of transfer is correctly described during initial plasticity (780–850 MPa) before unloading starts to occur at higher applied stresses. The effect of relaxation in the 10$\bar{1}$1, 11$\bar{2}$0 and 11$\bar{2}$2 grain families is relatively small, and correctly described in magnitude by the model. The behaviour of the 20$\bar{2}$1 grains which appear to be loaded, is captured more poorly by the model, though it is unclear to what extent this is due to a failure to describe the stiffness correctly. The relative elastic anisotropy of different lattice planes may be quite simply described as a function of the angle between their plane normal and the c-axis [28], but the corresponding plastic anisotropy resists such simple classification. The 0002 planes thus show a small degree of tensile plastic anisotropy, whereas the 10$\bar{1}$3 and 10$\bar{1}$2 planes show a larger degree of compressive plastic

anisotropy, while the $10\bar{1}1$ planes again show a small degree of tensile plastic anisotropy. The complexity of the response is due to the multiple deformation modes which are active. Some insight can be gained by considering the plastic intergranular strains, that is by carrying out a straight line fit to the elastic regime for each diffraction peak and calculating the difference between the observed strain and this linear fit. In general, for plane normals close to the a-axis, the intergranular plastic strains are tensile, whilst for those closer to the c-axis, but excepting the c-axis itself, the intergranular plastic strains are compressive. Fig. 3 shows these plastic intergranular strains for some lattice planes as a function of macroscopic plastic strain, highlighting the development with deformation. Thus, the 0002 lattice plane appears to saturate at a relatively low plastic strain, whereas the $11\bar{2}2$ saturates more slowly. Correspondingly the $10\bar{1}3$ and $10\bar{1}2$ planes appear not to have saturated at the macroscopic plastic strain reached in this test. Although the changes in strain in these latter two planes at higher macroscopic plastic strains are comparable to the uncertainty obtained from the peak fitting routine, the fact that the strain changes in the two planes agree so closely gives some strength to the argument that actual physical changes are being observed.

The strains measured in the transverse (perpendicular to the applied load) direction are shown in Fig. 4. Again the small elastic anisotropy results in relatively little difference in the elastic response of the various diffraction planes, but those differences that exist are well captured by the model. In contrast to cubic materials where measurements made parallel to the applied load are typically in better agreement with self-consistent model predictions than those made perpendicular to it [7], here the agreement is excellent for the various planes, with the exception of $11\bar{2}0$. The 0002 (basal) plane shows large load transfer effects, with increased compressive strains being observed, whereas the $10\bar{1}2$ and $10\bar{1}3$ planes show relatively small effects. The behaviour of these three peaks should be contrasted with the behaviour that is seen in the axial direction, where the 0002 plane shows little load transfer and it is the $10\bar{1}2$ and $10\bar{1}3$ planes which do. On the other hand, the prism $10\bar{1}0$ oriented grains show evidence of load transfer in both the transverse and axial directions. The remaining diffraction peaks show small intergranular strain accumulation in this direction.

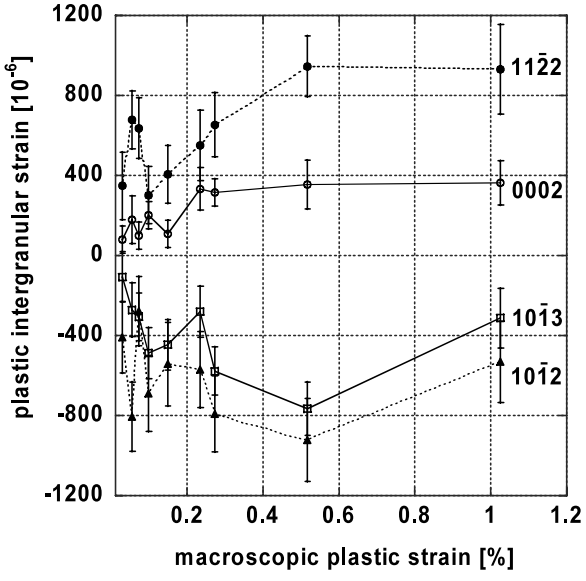

Fig. 3. Plastic component of single peak strains in the axial direction for some peaks plotted as function of macroscopic plastic strain.

5. Strains obtained from Rietveld refinement

The lattice parameter strains obtained from the Rietveld refinement are shown in Fig. 5. The strains obtained through analyses of the individual a and c lattice parameters are shown, as well as the average $(2\varepsilon_a+\varepsilon_c)/3$ as described in [10]. The compressive scale is three times as large as the tensile scale to highlight the variations between a and c. Even with this magnification, the splitting in the axial direction is much larger than in the transverse direction; while the low anisotropy does cause a noticeable split in the a and c axial strains, this is not observed in the transverse strains. The average strains in both the axial and transverse directions are remarkably linear. A straight line fit was applied to the elastic part (<750 MPa) of this average, in each direction, and the difference between this linear fit and the observed data is shown in Fig. 6; the transverse direction data are shown as open symbols and axial direction data as closed symbols. The data are plotted against both macroscopic stress and macroscopic plastic strain. These figures also include data using the 'constrained' fit proposed in [10]. In such a fit, the c:a ratio is fixed to be equal to the nominally unstressed reference value (i.e. at zero load here) throughout the fitting process. This is in contrast to the normal Rietveld refinement shown in Fig. 4 where the a and c lattice parameters are independent. As expected, the results of the constrained fit and the average from the normal fit are the same to within error for the two methods, although the data obtained via the constrained fit have a smaller uncertainty due to there being only a single fitting parameter rather than two. The plastic strains in Fig. 5 reach a maximum of around 200×10^{-6} at $\sim0.5\%$ plastic strain, with similar values seen in both the axial and transverse directions, before decreasing with further plasticity.

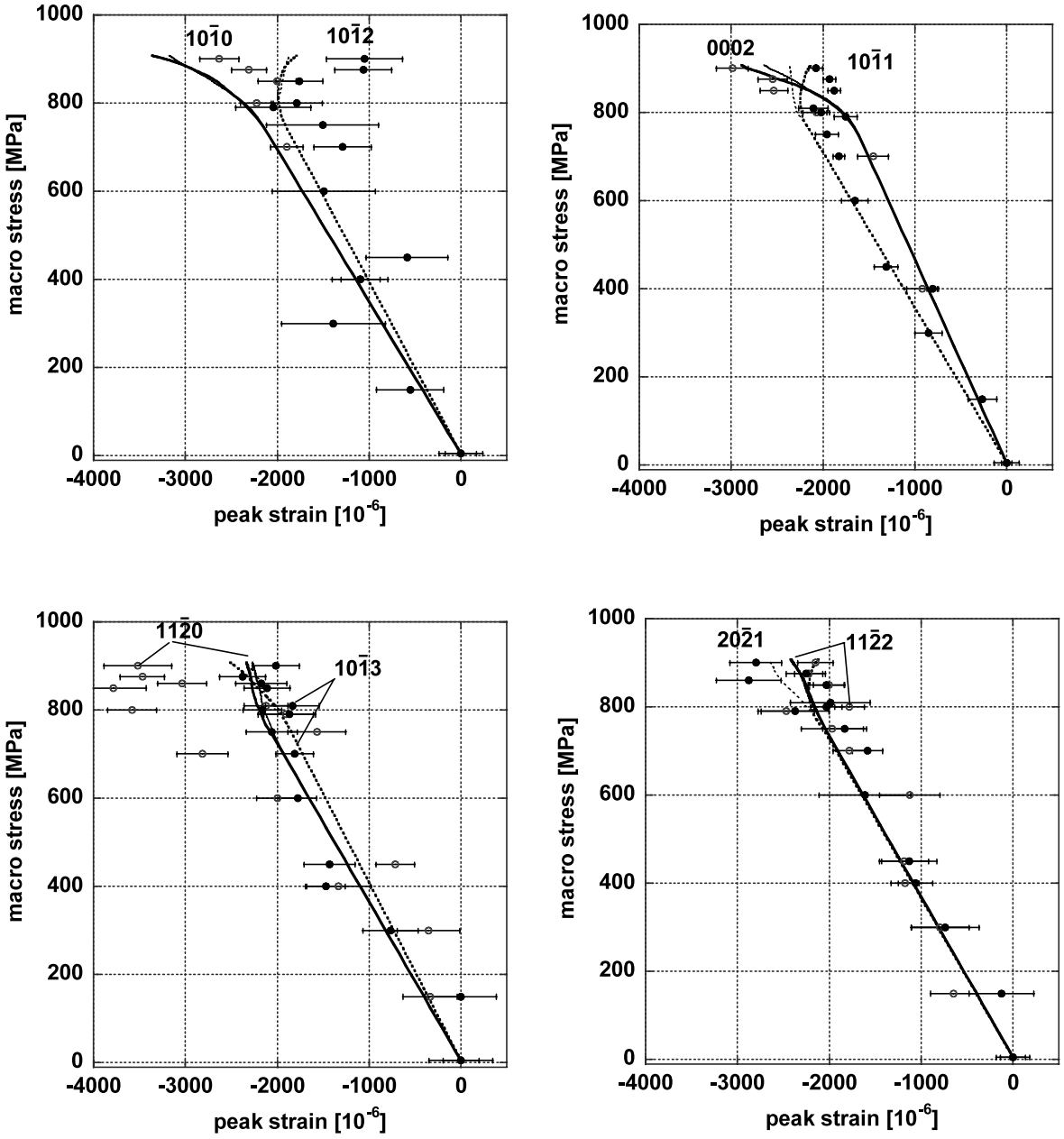

Fig. 4. Single peak transverse strains compared with model predictions. Thick lines are for the model run with four slip modes, the thin lines for the model run with three slip modes and three twinning modes.

6. Discussion

With the caveats already mentioned, the model does give good agreement with the experimental results, particularly in the transverse direction. The model predictions support the observation [22,23] that $\langle c+a \rangle$ slip is expected in preference to twinning. Further adjustments to the model fitting parameters can improve agreement to an even greater extent. For instance, it is possible for the model to predict that upon plasticity the 10$\bar{1}$2 and 10$\bar{1}$3 planes will unload in the axial direction, by choosing the various CRSS such that basal slip activates before prismatic and pyramidal slip. This does improve the agreement with the experimental data (see Fig. 3), but it is not supported by other experimental reports of the relative ease of different slip modes, as detailed in Section 3. Further, such a change to the model does not prevent the 0002 planes from unloading at high stresses. Such adjustments, which are possibly non-physical in nature, are not appropriate at this stage. On the other hand, the determination of ease of slip on different lattice planes which is reported in the literature are typically based on uniaxial loading of single crystals, and therefore, do not take into account the constraints and impurities which will affect a crystallite within the polycrystal alloy. It should also

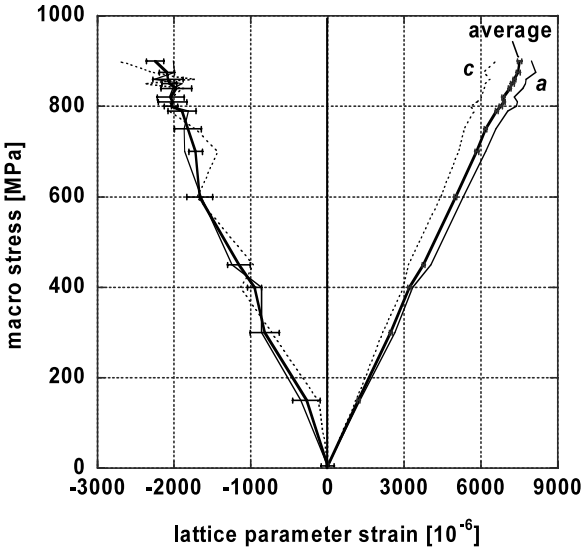

Fig. 5. Rietveld refinement determined strains, axial and transverse, for a (thin, continuous) and c (broken) lattice parameters. Note that the compressive strain axis has been expanded by a 3-fold compared with the tensile strain axis. Also shown is the average Rietveld strain (thick continuous with error bars; see Section 5).

be noted that the model does not include any processing induced strains, either from the forging deformation or from the heat treatment. However, these are likely to be small since (a) the slow air cool after the heat treatment is designed to produce low residual strains and (b) the loading behaviour of the individual planes shows no evidence of early yield; all the planes show linear behaviour below 750 MPa.

If one assumes an elastic unload from the data shown here (i.e. Fig. 3), good agreement is obtained with the data presented by Cho et al. [8] for the residual strains following unloading from a comparable plastic strain, with two exceptions. Firstly, in the axial direction Cho shows a small ($\sim 200 \times 10^{-6}$) compressive residual strain for the 0002 plane, whereas the data here would suggest a tensile strain $\sim 350 \times 10^{-6}$ (Fig. 3b). Secondly, in the transverse direction Cho shows a more significant compressive strain ($\sim 300 \times 10^{-6}$) for the $10\bar{1}3$ plane, whereas the data here suggests a small but tensile residual strain. These appear to be the only qualitative changes in the lattice strains due to the reverse yielding seen in the macroscopic response, although of course some more subtle changes in magnitude if not in sign may also occur for other planes. Due to a lack of available experimental time, it was not possible to carry out measurements of residual strains during the test described here. The model predicts a completely elastic unload, requiring the system to be driven into compressive loading before reverse yielding occurs. It, therefore, seems likely that the reverse yield may in fact be complicated by factors not included in the model, perhaps dislocation recombination [17]. To explore this question would require a considerably more detailed experimental investigation, which should most obviously include a comparison between tensile and compressive loading tests, since this will also explore any contributions from twinning modes.

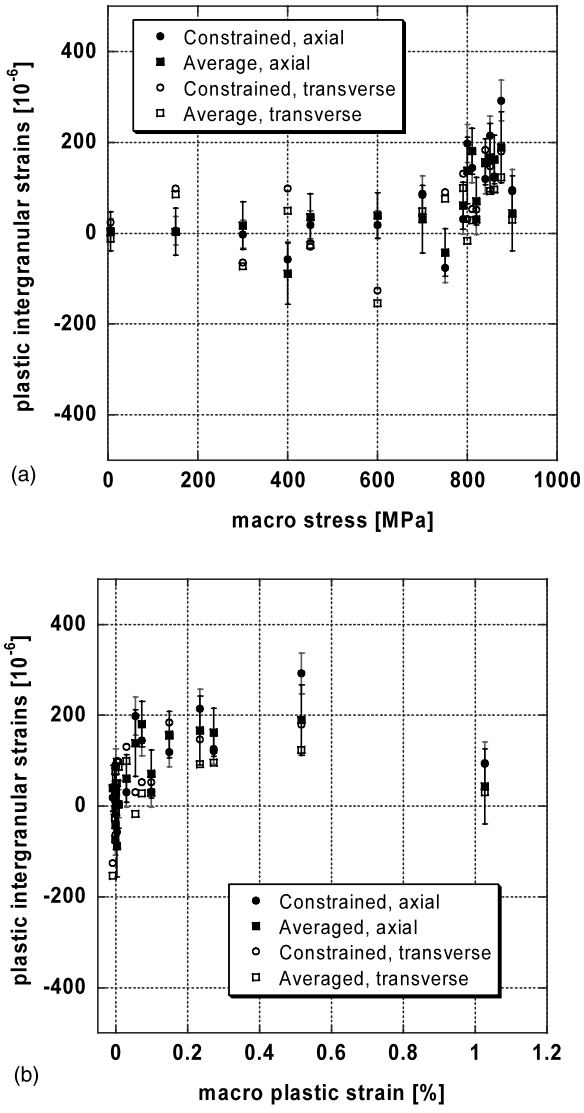

Fig. 6. Plastic component of strain determined by Rietveld refinement, plotted as function of (a) macroscopic applied stress and (b) macroscopic plastic strain.

The Young's moduli and Poisson's ratios determined macroscopically in the elastic regime and from the Rietveld refinement of the diffraction data are listed in Table 2. As can be seen, there is excellent agreement between all the various determinations of both the Young's modulus and the Poisson's ratio. The values collected here, along with the linearity throughout the plastic regime in both the axial and transverse directions (shown in Fig. 5) are extremely reassuring. This demonstrates that it is appropriate to use strains determined from Rietveld refinement parameters for engineering strain scanning measurements. Further, the appropriate modulus to use is the macroscopic modulus.

Table 2
Measured and modelled macroscopic parameters

	Modulus (GPa)	Poisson's ratio
Macroscopic, literature [29]	120	0.31
Macroscopic, measured	119.4 ± 1.1	–
Macroscopic, model	120.5	0.30
Rietveld refinement, average	119.6 ± 1.0	0.31 ± 0.1
Rietveld refinement, constrained	120.4 ± 0.8	0.31 ± 0.1

The worst case discrepancy in making this assumption, based on the strains shown in Fig. 6 for a macroscopic plastic strain of 0.5%, corresponds to an error in stress of only ~ 25 MPa. The corresponding error resulting from the use of just a single diffraction peak could be as much as five times this value. Careful choice of a single lattice plane for such measurements will reduce the error, but such a choice is made more problematic since those planes which are linear in the axial direction are not linear in the transverse direction, and vice versa, with the exception of the $11\bar{2}2$ plane which does seem to produce low intergranular strains in both sample directions. The different degree of non-linearity in the two directions would cause problems in the case of non-uniaxial loading. The data presented here gives a strong case for the use of Rietveld refinement for strain determination by neutron diffraction in this material, at least in untextured systems. In a textured material, the macroscopic modulus will be weighted by the dominant texture. Correspondingly however, the Rietveld refinement will be weighted more strongly to the more intense diffraction peaks, which result from the texture, and hence the strain response will be modified accordingly. It is likely, therefore, that the technique would remain valid, although a more systematic study would be appropriate.

7. Conclusions

Neutron diffraction data has been collected, showing the strain evolution for different diffraction peaks in the alpha titanium alloy IMI 834 under applied stress. Good agreement is obtained between experimental data obtained in the axial direction and a self-consistent model including four slip modes; excellent agreement is found for the transverse direction. The reverse yielding observed in the macroscopic stress strain curve is found to have only a small effect on the intergranular strains measured experimentally, and is not predicted by the model. Strains determined from a Rietveld refinement of the diffraction data have been shown to be appropriate to use when performing engineering strain scanning measurements, with only small deviations from linearity in the plastic regime. The appropriate modulus to employ in such cases is the macroscopic modulus.

References

[1] D.J. Fray, J. Miner. Metals Mater. Soc. 53 (10) (2001) 26–31.
[2] M.R. Daymond, N.W. Bonner, Physica B (2002), submitted for publication.
[3] J.R. Cho, S.M. Roberts, R.C. Reed, K.T. Conlon, in: M. Winstone (Ed.), Titanium Alloys at Elevated Temperature: Structural Development and Service Behaviour, Institute of Materials, London, 2001, pp. 151–164.
[4] J.W.L. Pang, G. Rauchs, P.J. Withers, N.W. Bonner, E.S. Twigg, J. Neutron Res. 9 (2–4) (2001) 373–379.
[5] I.C. Noyan, J.B. Cohen, Residual Stress-Measurement by Diffraction and Interpretation, Springer, New York, 1987.
[6] S.R. MacEwen, J. Faber, A.P.L. Turner, Acta Metall. 31 (5) (1983) 657–676.
[7] B. Clausen, T. Lorentzen, M.A.M. Bourke, M.R. Daymond, Mater. Sci. Eng. 259 (1) (1999) 17–24.
[8] J.R. Cho, D. Dye, K.T. Conlon, M.R. Daymond, R.C. Reed, Acta Mater. (2002), submitted for publication.
[9] M.R. Daymond, M.A.M. Bourke, R.B. Von Dreele, B. Clausen, T. Lorentzen, J. Appl. Phys. 82 (4) (1997) 1554–1562.
[10] M.R. Daymond, M.A.M. Bourke, R.B. Von Dreele, J. Appl. Phys. 85 (2) (1999) 739–747.
[11] C.G. Windsor, Pulsed Neutron Scattering, Taylor & Francis, London, 1981.
[12] H.M. Rietveld, J. Appl. Crystallogr. 2 (1969) 65–71.
[13] M.R. Daymond, H.G. Priesmeyer, Acta Mater. 50 (6) (2002) 1613–1626.
[14] P.A. Turner, N. Christodoulou, C.N. Tomé, Int. J. Plasticity 11 (3) (1995) 251–265.
[15] R. Hill, J. Mech. Phys. Sol. 13 (1965) 89–101.
[16] J.W. Hutchinson, Proc. R. Soc. London A319 (1970) 247–272.
[17] T. Lorentzen, M.R. Daymond, B. Clausen, C.N. Tomé, Acta Mater. 50 (6) (2002) 1627–1638.
[18] M.A. Gharghouri, C.N. Tomé, J. Root, ICOTOM-12, NRC Press, Ottawa, 1999.
[19] E.A. Brandes, G.B. Brook (Eds.), Smithells Metals Reference Book, seventh ed., Butterworth/Heinemann, Oxford, 1992.
[20] A.T. Churchman, Proc. R. Soc. 226A (1954) 216–226.
[21] A. Akhtar, Metall. Trans. 6A (1975) 1105–1113.
[22] D.J. Bacon, J. Vitek, Met. Mater. Trans. 33A (2002) 721–733.
[23] J.C. Williams, R.G. Baggerly, N.E. Paton, Met. Mater. Trans. 33A (2002) 837–850.
[24] M.R. Daymond, Physica B 301 (3–4) (2001) 221–226.
[25] B.E. Warren, X-Ray Diffraction, Dover, New York, 1990.
[26] U.F. Kocks, C.N. Tomé, H.-R. Wenk, Texture and Anisotropy, Cambridge University Press, Cambridge, 1998.
[27] T.W. Clyne, P.J. Withers, An Introduction to Metal Matrix Composites, Cambridge University Press, Cambridge, 1993.
[28] J.F. Nye, Physical Properties of Crystals, Oxford University Press, Oxford, 1992.